PCCP

Accepted Manuscript

ROYAL SOCIETY OF CHEMISTRY

rsc.li/pccp

View Article Online
DOI: 10.1039/C7CP06612K

Journal Name

ARTICLE TYPE

Cite this: DOI: 10.1039/xxxxxxxxxx

Ubiquitous deprotonation of terephthalic acid in the self-assembled phases on Cu(100)

B. Quiroga Argañaraz, [a] L. J. Cristina,[a,‡] L.M. Rodríguez, [a] A. Cossaro, [b] A. Verdini, [b] L. Floreano, [b] J.D. Fuhr, [a] J. E. Gayone, [a] and H. Ascolani. [a]

Received Date
Accepted Date

DOI: 10.1039/xxxxxxxxxx

www.rsc.org/journalname

We performed an exhaustive study of terephthalic acid (TPA) self-assembly on the Cu(100) surface, where first-layer molecules display two sequential phase transitions in the 200 - 400 K temperature range, corresponding to different stages of molecular deprotonation. We followed the chemical and structural changes by means of high-resolution X-ray photoelectron spectroscopy (XPS) and variable-temperature scanning tunneling microscopy (STM), which were interpreted on the basis of density functional theory (DFT) calculations and photoemission simulations. In order to disentangle the spectroscopic contribution of molecules in different states of deprotonation, we modified the substrate reactivity by deposition of a small amount of Sn, which hampers the deprotonation reaction. We found that the characteristic molecular ribbons of the TPA/Cu(100) α-phase at low temperature contain a significant fraction of partially deprotonated molecules, contrary to the expectation of a fully protonated phase, where the self-assembly was claimed to be simply driven by intermolecular double hydrogen bonds $[OH\cdots O]$. On the basis of our simulations, we propose a model where the carboxylate groups of the partially deprotonated molecules form single hydrogen bonds with the carboxylic groups of fully protonated molecules. By real time XPS, we also monitored the kinetics of the deprotonation reaction. We show that the network of mixed single and double hydrogen bonds inhibits further deprotonation up to ~ 270 K, whereas isolated molecules display a much lower deprotonation barrier.

1 Introduction.

Benzyl-carboxylic acids are widely used as synthons in the generation of two-dimensional (2D) hetero-organic architectures at surfaces.[1–5] On surfaces, carboxyl groups form different types of bonds including hydrogen bonds, carboxylates and metal-ligand bonds, giving rise to a variety of self-assembly mechanisms and structures. In this context, fundamental studies of benzyl-carboxylic acids adsorbed on metallic surfaces with focus on the deprotonation reaction itself and also on its consequences on the stabilization of new structures have got renewed relevance.[6–18]

Terephthalic Acid (TPA) is a prototype case of the above mentioned family of molecules and its adsorption and self-assembly properties, either alone[7–13] or coadsorbed with different metallic atoms,[3,19] have been studied on different surfaces. In particular, the TPA/Cu(100) system has been recognized as a model case to investigate the effects of deprotonation on the molecular interactions and the resulting self-assembly structures,[8,12] because the adsorbed molecule can assume either single or double deprotonation of its two carboxylic terminations. For any given coverage below one monolayer (ML), the TPA/Cu(100) system forms three different structural phases depending on the substrate temperature, namely α, β and γ, all of them with the molecules adsorbed flat on the surface. The α-phase is obtained by depositing the molecules at low temperatures (LT, $\sim$200K) and is stable up to $\sim$270K, where it transforms into the β one. The latter is metastable and gradually transforms into the γ-phase at room temperature (RT), which is stable up to 400 K. It is well established that molecules in the γ-phase are arranged into a commensurate (3×3) superlattice composed of fully deprotonated molecules. The β-phase displays a $(9\sqrt{2}\times 2\sqrt{2})R45^\circ$ symmetry composed of a mix of fully deprotonated and semiprotonated molecules.[12] The α-phase was attributed to complete (i.e. protonated) TPA molecules although, however, it has been scarcely investigated and its nature is not completely understood.

Searching for new methods of tailoring the formation of

[a] Centro Atómico Bariloche, CNEA, Av. E. Bustillo 9500, R8402AGP, Bariloche, Argentina. E-mail: gayone@cab.cnea.gov.ar, ascolani@cab.cnea.gov.ar
[b] CNR-IOM, Laboratorio TASC, Basovizza SS14 Km. 163.5, I-34149 Trieste, Italy.
† Electronic Supplementary Information (ESI) available. See DOI: 10.1039/b000000x/
‡Present address: Instituto de Física del Litoral (IFIS Litoral), CONICET. Gral. Güemes 3450, S3000GLN Santa Fe, Argentina.

View Article Online
DOI: 10.1039/C7CP06612K

supramolecular networks on surfaces, we oriented our efforts to the investigation of surface alloys as a route for tuning the molecule/surface interactions. Recently, we showed that the modification of the bare Cu(100) substrate by Sn alloying causes a strong reduction of the reactivity of the surface with respect to the carboxyl groups of TPA molecules. Furthermore, deprotonation is completely inhibited on the $(3\sqrt{2}\times\sqrt{2})R45^\circ$ reconstruction[20,21] of the 0.5 ML Sn/Cu(100) phase (hereafter $3\sqrt{2}$) and the molecules form 2D sheets[13] similar to those observed on the Au(111) substrate[7].

In this work, we compare the adsorption and self-assembly properties of the TPA/Cu(100) system with those of TPA molecules adsorbed on the Cu(100) surface modified with a very small amount of predeposited Sn, which is shown to be sufficient for decreasing the Cu reactivity, but preserving its surface structure and symmetry. We thus performed a thorough study of the LT α -phase in the TPA/Cu(100) system by means of Scanning Tunneling Microscopy (STM), X-ray Photoemission Spectroscopy (XPS), and Functional Density Theory (DFT) calculations. In contrast with previous report, we show that the α-phase is not a pure protonated phase, but a mix of protonated and semiprotonated TPA molecules. Finally, we compared the kinetics of the deprotonation reaction on the two substrates by following the amount of carboxylates with increasing temperature.

We show that the Cu(100) surface reactivity is larger than expected, being capable of catalyzing the partial deprotonation of TPA at low temperature. Moreover, we propose a model where the semi-protonated molecules are incorporated in the α phase through the formation of single hydrogen bonds $[OH\cdots O]$.

2 Methods

2.1 Experimental Methods

Three independent ultrahigh vacuum systems were used to perform the experiments involved in this work. The STM experiments were carried out at the Centro Atómico Bariloche, in Bariloche, Argentina, while the XPS experiments with synchrotron radiation (SR) were carried out at the ALOISA beam line[22,23] of the ELETTRA synchrotron in Trieste, Italy. In addition, complementary XPS experiments were carried out in Bariloche by using a SPECS system with monochromatized Al K_α radiation in order to check reproducibility. The three vacuum chambers have a base pressure in the low 10^{-10} mbar range.

The STM system is from Omicron Nanotechnology and is basically equipped with a variable-temperature STM (model AFM/STM VT 25 DRH), a LEED optics and a homemade ion gun for Ar^+ sputtering. All the reported STM images were taken with W tips. Negative sample bias voltages correspond to occupied-states images. The thermal drift was compensated during the measurements by applying the facility provided by the MATRIX software used to control the STM.

In the STM chamber, the Cu(100) surfaces were prepared by cycles of sputtering at 1.5 keV and annealing at 770 K. Sn atoms were evaporated from a homemade Knudsen cell onto clean Cu(100) surfaces at a rate of 0.1 ML every 2.5 min approximately, as follows from the calibration obtained from the LEED patterns of the Sn/Cu(100) system aforementioned RT reconstructions.[20] The quality of the clean Cu(100) substrate and the $3\sqrt{2}$ reconstruction was checked by LEED (see Supplementary Information (SI), section S1).

The TPA molecules (Sigma Aldrich, 98% purity) were used as received. The molecules were evaporated from a resistively-heated boron nitride crucible at a rate of about 0.1 monolayer (ML) per minute. We define 1 ML as the surface coverage corresponding to the (3×3) phase, that is, a molecular coverage of 1 TPA molecule per 9 Cu atoms in the top surface layer. In the STM chamber, the adsorption at LT were performed as follows. The substrate was cooled by means of the continuous-flow cryostat associated to the STM working with liquid nitrogen. Temperatures were measured by using a Si diode that is located close to the sample on the clamp of the cold finger. At thermal equilibrium, the sample temperature is estimated to be 15K higher than the Si diode reading. This correction was considered all along this article. Once the sample reached the desired temperature (T_{STM}), it was disconnected from the cold finger and moved in front of the evaporator for TPA dosing. After the evaporation, the sample was connected again to the cold finger. From previous experiments,[24] we estimated a maximum temperature drift of 50 K. The preparation temperatures in the STM chamber are thus evaluated as $(T_{prep} = T_{STM} + 50K)$, which should be regarded as an upper value.

In ALOISA the clean Cu(100) surface, the $3\sqrt{2}$ reconstruction as well as the 3×3 phase, were verified by reflection high-energy electron diffraction (RHEED). The SR-XPS data were obtained by use of a p-polarized X-ray beam at grazing incidence (about 4°). The spectra, taken with a photon energy of 655 eV, were measured in normal emission by means of a hemispherical electron analyser with angular acceptance of 2° and an overall energy resolution of 300 meV. The Binding Energy (BE) scale of the analysed experimental spectra was calibrated by setting the BE position of the $Cu3p_{3/2}$ line to 75.0 eV. The experimental O1s XPS spectra were fitted with Voigt functions and Shirley-type backgrounds. A Lorentzian width of 0.15 eV was used in all cases. Four energy windows, centered on the regions of the Fermi edge and the Cu3p, C1s, and O1s core levels, were typically acquired by means of a 2D delay-line detector.[25] The evolution of the amount of carboxylates with increasing temperature was obtained by monitoring the corresponding O1s core level throughout sample annealing in snapshot acquisition mode. This mode requires a lower kinetic energy resolution (600 meV) to collect the whole core level peak profile within a single shot (2 sec) of the 2D detector. At ALOISA the sample temperature was monitored by means of a thermocouple in direct contact with a Mo spacer below the sample.

2.2 Theoretical Details

First-principles electronic structure calculations were performed within the DFT framework using the Quantum-espresso plane-wave code[26]. To take into account van der Waals interactions, we used the revised VV10 nonlocal exchanged-correlation density functional[27,28]. For the surface calculations we used the slab method, with four layers representing the surface and a vacuum

View Article Online
DOI: 10.1039/C7CP06612K

size of ∼10 Å. Except for the two lower layers that were kept fixed at the bulk distance, all the atoms in the cell were allowed to relax. Residual forces on the atoms after geometric relaxation were smaller than 10^{-3}Ry/a_0. We used ultrasoft pseudopotentials with an energy cut-off of 30 Ry. Brillouin integrations were done using grids equivalent to $12 \times 12 \times 1$ for a $(\sqrt{2} \times \sqrt{2})R45°$ unit cell. Core-level shifts for oxygen atoms are obtained as total energy differences between calculations performed with one of the oxygen atom using a 1s core-hole pseudopotential.

3 Results

3.1 Characterization of the α-phase.

A representative image of the TPA/Cu(100) α-phase prepared at a substrate temperature of 230 K is shown in Figure 1, where the molecules are observed to grow by self-assembly into ribbons oriented at $\pm(9° \pm 2°)$ with respect to the $< 100 >$ crystallographic directions of the substrate, in full agreement with the observations of Stepanow et al.[8]. Equivalent images were obtained at 180 K. A characteristic of the α-phase ribbons is a long wavelength modulation of the molecular apparent height, as clearly seen in Figure 1, which gives a striped appearance to the ribbon surfaces. The latter stripes (indicated with blue dashed lines in the image) are oriented at $\pm(29° \pm 2°)$ with respect to the growth direction of the ribbons. The molecular network of the α phase presents an intermolecular distance along directions $\vec{b_1}$ or $\vec{b_2}$ of (7.3 ± 0.5) Å (see the inset of the figure); the corresponding subtended angle is $(78° \pm 3°)$. The intermolecular distance along the growth direction of the α phase, $(\vec{b_2} - \vec{b_1})$, is (9.5 ± 0.5) Å, which we have seen to match very well that of the 2D sheets formed by complete protonated molecules on the $3\sqrt{2}$ reconstruction.[13]

In order to understand the chemical state of TPA in the α-phase, we compared the high resolution XPS of the O1s and C1s peaks with those measured in different phases and substrates at the same coverage of the sample shown in Figure 1. In particular, we considered the (3×3) TPA/Cu(100) γ-phase and the LT phase of TPA on Sn-alloyed Cu(100) surfaces. The O1s spectrum corresponding to the (3×3) phase, with a single peak at a BE of 531 eV (upper panel of Figure 2), is a reference spectrum for terephthalates,[11,12] corresponding to a film made only of fully depronated molecules.

On the contrary, the O1s spectrum corresponding to the TPA on $3\sqrt{2}$-Sn/Cu(100) system (shown at the bottom of the middle panel of Figure 2) can be considered a reference spectrum of 2D sheets of protonated TPA molecules connected through straight double $[OH \cdots H]$ bonds[13]. This spectrum can be fitted with two main components separated by 1.31 eV,[29,30] where the one at lower BE (532.08 eV) is originated in the CO group, and that at higher BE is originated in the OH group. Although displaying a similar spectral weight, the OH peak is systematically broader than the CO one, as previously reported also for benzoic acid on Au(111).[29,30] The spectrum of the TPA sheets grown on the $3\sqrt{2}$ reconstruction is practically equal to that obtained for a multilayer grown at low temperature (lower panel), apart from a rigid shift of 0.5 eV to lower BEs due to the surface screening by the metal substrate. The reduction of the Sn coverage from 0.5 to 0.1 ML does not cause qualitative changes in the line shapes beyond a slight increment of the shoulder at 531 eV corresponding to therephthalates.

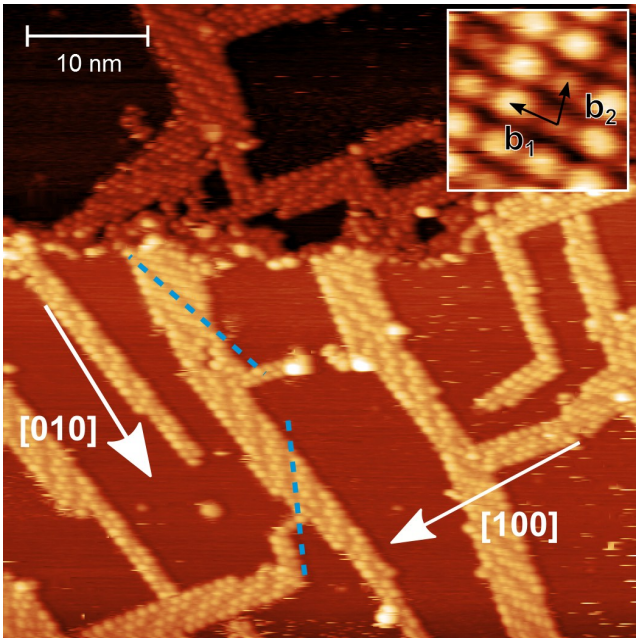

Fig. 1 STM image of the LT α-phase of TPA/Cu(100) at a molecular coverage of 0.4 ML. Surface prepared at ∼230K and imaged at 180K (-2V/300 pA). The substrate main symmetry directions are indicated by the white arrows, while the dashed blue lines highlight the orientation of the supra-molecular striped modulation for two domains, which are mirror-symmetric with respect to the [010] direction. The inset shows a high resolution image of the ribbons were the molecular arrangement can be clearly seen.

The O1s peak of the α-phase looks significantly different from that of the TPA/$3\sqrt{2}$ system. Apart from the prominent shoulder at ∼531 eV, the O1s peak presents a dominant component at ∼532.5 eV. The corresponding C1s spectrum presents a characteristic double peak in the BE region (284 to 285 eV) associated to the carbon atoms of the benzene rings, which is not seen in the other spectra. Thus, both the O1s and the C1s core-level spectra corresponding to the α-phase are not consistent with the common assumption of a fully protonated phase. In a previous work, Stepanow *et.al.*[8] had fitted the O1s peak corresponding to the α-phase with two components, and had associated the ribbons with a structure containing only protonated molecules forming double hydrogen bonds $[OH \cdots O]$. However, a careful inspection of the O1s and C1s spectra presented by Stepanow *et.al.*[8] reveals that they are similar to the present ones of the α-phase, but they are smeared by a combination of poor resolution and low signal to noise ratio (although the characteristic splitting of the benzene carbon peak can be easily recognized below the single peak fitting curve in Fig. 2 of Ref.[8]).

As a first attempt to rationalize the chemical state of TPA in the α-phase, we first tried to fit the O1s spectrum by a linear combination of a doublet corresponding to the protonated molecule (with fixed intensity ratio) and one peak corresponding to a deprotonated TPA, as obtained from the reference spectra of the

View Article Online
DOI: 10.1039/C7CP06612K

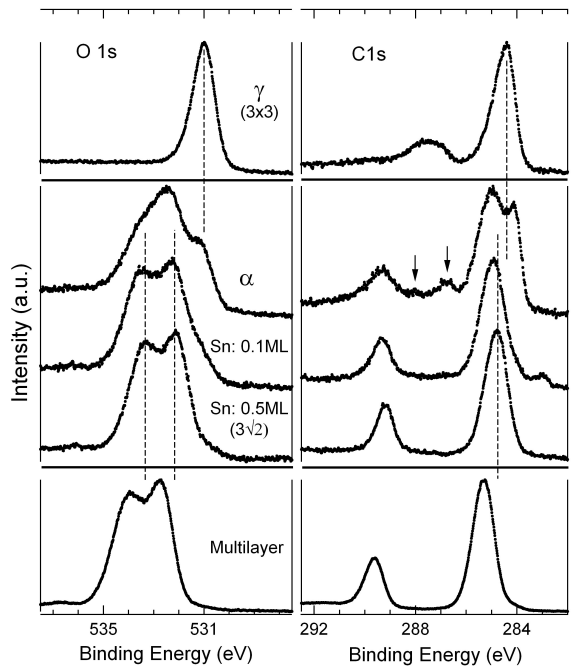

Fig. 2 Comparison of representative O1s and C1s photoemission spectra of TPA films adsorbed on different substrates. Upper Panel: typical spectra of the (3×3)-TPA/Cu(100) phase, as obtained after annealing to 400 K. Middle panel: representative spectra of TPA films obtained by depositing ∼0.4ML of TPA at ∼230 K on the Cu(100) surface and two Sn/Cu(100) alloys with increasing Sn content: top curve, the TPA/Cu(100) LT α-phase, with a coverage determined from the spectrum of (0.38 ± 0.05); middle curve, TPA adsorbed on the 0.1ML Sn/Cu(100) alloyed surface, with coverage of (0.38 ± 0.05); bottom curve, TPA adsorbed on the 0.5ML Sn/Cu(100) alloyed surface (the $3\sqrt{2}$ reconstruction), with coverage of (0.34 ± 0.05). Lower panel: XPS spectra obtained from a multilayer of TPA molecules grown on a Cu(100) surface kept at ±230K. Notice that the latter O1s spectrum shows a small component at 536.8eV that we attribute to a shake-up satellite; consistently, this component is observed also in the films grown on the passivated Sn/Cu(100) alloyed surfaces.

TPA/$3\sqrt{2}$-Sn/Cu(100) and (3×3)-TPA/Cu(100) phases respectively. Even relaxing the constraints on peak width and position, this combination yields a clear mismatch with the measurements. The analysis of the difference spectrum (see SI, section S3) reveals the need of extra components accounting for a residual intensity larger than 10%. We performed careful analysis and supplementary measurements in order to exclude any possible influence of either surface defects or contaminants. Furthermore, the STM images of this interface indicate that the large majority of the adsorbed molecules are located in the α-ribbons (see SI, section S2, for a quantitative analysis). Therefore, the deprotonated contribution to the O1s spectrum should stem from molecules in the molecular ribbons. We remark that the C1s to O1s ratio of the peak areas (after correction by the cross-section) corresponds to the expected 1 to 2 stoichiometry. In addition, we verified that the line shapes of both the O1s and the C1s are highly reproducible on different Cu(100) samples, different experimental chambers and different spectroscopic instrumentation (see SI, section S4), therefore they must be related to intrinsic properties of the TPA/Cu(100) system prepared at LT.

At a first glance, an additional contribution to the O1s line is clearly needed between the OH and the CO components at a BE of ∼532.5 eV. We can exclude that this extra contribution may correspond to a carboxylate (COO^-) bound at undercoordinated sites. In fact, this component is shifted by ∼1.5 eV to higher BE from the carboxylate peak, whereas the coordination of carboxylates to Cu adatoms has been reported to yield a shift by only +0.6 eV for the case of Fe-TPA metal-organic networks on Cu(100) [31], and no shift for TPA on Cu(110) [11]. Therefore, we tentatively assign this extra component to a OH peak shifted to lower BE by ∼0.8 eV.

3.2 Model for the carboxyl/carboxylate interaction in the α-phase.

In order to determine the molecular configurations that can give rise to this extra OH peak, we performed DFT based simulations of core-level shifts for the most plausible scenarios. We considered the following four possibilities: (I) paired carboxyl groups adsorbed at inequivalent adsorption sites of the surface, i.e. molecules in different registry with the substrate; (II) unpaired carboxyl groups, i.e. not forming $[OH\cdots O]$ bonds with other carboxyls; (III) carboxyl groups interacting with ad-atoms or steps; (IV) carboxyl groups connected to a carboxylate by a single $[OH\cdots O]$ bond. We analysed these scenarios assuming a model based on two interacting molecules adsorbed on the Cu(100) surface. In each case, after relaxation, we simulated the O1s core level shifts, taking as reference the corresponding one of the deprotonated TPA molecule in the 3×3 adsorption geometry. The O1s spectra were then simulated by convolution of the calculated discrete lines with a gaussian function.

The first scenario can be easily discarded because the variation of the adsorption site yields shifts of the OH and CO components within 0.1 eV (see SI, section S5, for details). The scenario (II) is represented in Figures 3(a) and 3(b), where each TPA molecule has one of the carboxyl groups forming a double $[OH\cdots O]$ bond, while the other one is unpaired, as indicated by yellow and blue circles, respectively. Figure 3(c) compares the simulated peaks corresponding to the oxygen atoms involved in the double $[OH\cdots O]$ bond (orange line) with those of the unpaired carboxyl group (blue line). According to this simulations, the unpaired carboxyl group presents a significantly larger separation between OH and CO components (2.2 eV) than the corresponding ones forming the double $[OH\cdots O]$ bond (1.51 eV). This is in qualitatively agreement with experimental observations in the gas phase, where carboxyl groups are reported to be separated by 2.1 eV,[29] as compared with the 1.31 eV separation obtained for the O1s spectra of the multilayer and the TPA/$3\sqrt{2}$ surface alloy (Figure 2). In addition, the unpaired OH peak would be shifted to higher BE by ∼0.3 eV that is in the opposite direction of the required extra peak. The structural calculations reveal that there is a rotation of the unpaired carboxyl groups which brings the carbonyl (hydroxyl) closer (farther from) to the surface (see side view in Figure 3(b)), which very likely contributes to the increase of the calculated energy separation. We can then discard that unpaired carboxyl groups contribute to the 532.5 eV peak.

View Article Online
DOI: 10.1039/C7CP06612K

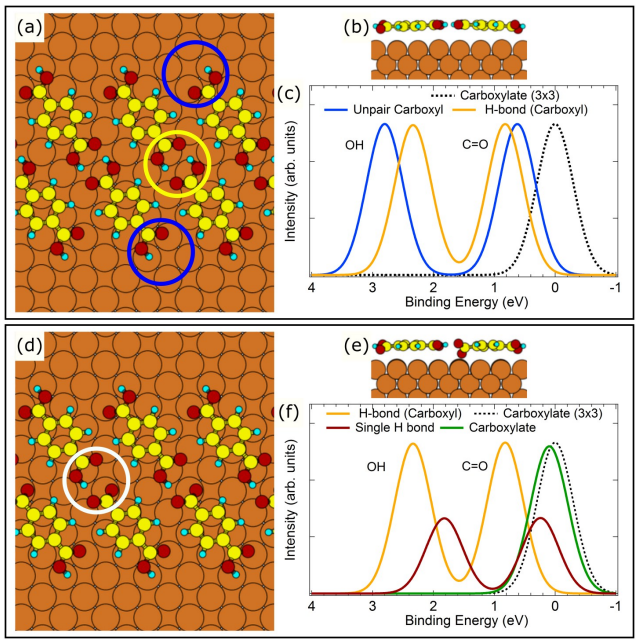

Fig. 3 Upper panel: top (a) and side view (b) of the relaxed structure for two TPA molecules forming a double $[OH\cdots O]$ bond. (c) Blue and orange lines correspond to the simulated O1s core-level photoemission spectra for the structure shown in (a). Lower panel: top (d) and side view (e) of the relaxed structure for two TPA molecules connected through a single $[OH\cdots O]$ bond. (f) Red and Green lines correspond to the simulated O1s core-level spectra related with the single $[OH\cdots O]$ bond (white circle in (d)), The orange line corresponding to a double $[OH\cdots O]$ shown in (c) is also included in (f). The simulated spectrum obtained for a deprotonated TPA molecule in a (3×3) adsorption geometry is included in (c), and (f) for comparison (dotted line).

To theoretically evaluate the possibility that a fraction of the molecules can interact with surface defects, we have added two Cu ad-atoms close to one of the unpaired carboxyl groups (see SI, section S6) that should give a good estimation of the chemical shifts due to interaction with steps, ad-atoms, or step-kinks. We found a shift of ∼0.15 eV to lower energy with respect to that of the paired $[OH\cdots O]$ bonds that, although going in the desired direction, it is quantitatively too small when compared to the required shift of -0.8 eV to account for the extra component at ∼532.5 eV. We note that this conclusion is in excellent agreement with the STM measurements on the LT phase of TPA/Cu(100), which show only a few molecules decorating the surface steps (see SI file, section S2).

The scenario (IV) is shown in Figures 3(d) and 3(e), representing the possibility that a fraction of the TPA molecules in the α-phase is partially deprotonated. Starting from the configuration (II) of Fig. 3(a), we deprotonated one of the paired carboxyl groups, otherwise connected with a double $[OH\cdots O]$ bond. After relaxing the geometry of this configuration, we found that the carboxyl/carboxylate interaction is stabilized by a single $[OH\cdots O]$ bond (white circle in Figure 3(d)). In this configuration, one of the O atoms of the carboxylate group is displaced downward, getting very close to the Cu atoms, while the other one is displaced slightly upward (see Figure 3(e)). Remarkably, the intermolecular distance obtained for the single $[OH\cdots O]$ bond is very similar to that obtained for the double $[OH\cdots O]$ bond of Figure 3(a) (9.8 Å and 9.7 Å respectively). Figure 3(f) compares the simulated O1s spectra of the carboxyl (red line) and carboxylate (green line) groups that are paired by the single $[OH\cdots O]$ bond. In spite of being chemically inequivalent, the O atoms of the carboxylate give rise to O1s peaks with similar BEs, which result in one single peak (green line) very close to the carboxylate position of the (3×3) phase (dotted line). In this case, the calculations predict a large chemical shifts to lower binding energy of the OH and CO components involved in the single $[OH\cdots O]$ bond. In particular, the OH peak is shifted by -0.5 eV in reasonable agreement with the shift of -0.8 eV required to account for the extra component at 532.5 eV. The corresponding CO peak is shifted by 0.6 eV to a BE position very close to the carboxylate peak.

Therefore, from the analysis of the different configurations, we propose that the origin of the complex shape of the O1s line is the formation of single $[OH\cdots O]$ bonds between carboxylic and carboxylate groups facing one another. In order to test the proposed model, we built a fitting function with five peaks and applied it to the analysis of the experimental O1s spectra related to the α-phase of TPA/Cu(100) and to the LT phase of TPA on the Sn-alloyed surfaces. Four peaks account for the OH and the CO groups of the double and single $[OH\cdots O]$ bonds (orange and red lines in Figure 3(f)), and the fifth one for the carboxylate of the single $[OH\cdots O]$ bond (green line). According to the model, the areas of the three components associated to the single H bonds are correlated: the ratio of the area of the carboxylate peak, to the area of the CO peak and to the area of the OH peak must be 2:1:1. This condition was imposed to the fitting function.

Figure 4 and Table 1 show the fitting results for the three O1s spectra shown in the middle panel of Fig. 2. We start the analysis from the O1s spectrum of the TPA/3$\sqrt{2}$-Sn/Cu(100) film (bottom) that can be fitted with two main components separated by 1.31 eV plus a minor component, ∼ 3%, associated with carboxylates. Regarding the TPA film on the 0.1ML-Sn/Cu(100) surface alloy (middle), the fitting results only show a small increment of carboxylates. This finding indicates that a very low Sn amount is sufficient to eliminate the complexities from the O1s line of the α-phase (top) of TPA/Cu(100). However, the corresponding C1s line shows small additional peaks to the two main ones associated to the fully protonated molecules. Clearly, the additional peaks are related to the component at 531 eV and, therefore, they should be originated in the terephthalates adsorbed (with unknown configurations) on the surface.

For the α-phase of TPA/Cu(100), the peak shape from the protonated CO and OH paired by a double bond is very close to the one used to fit the TPA/3$\sqrt{2}$-Sn/Cu(100) film, apart from a small decrease of the BE separation between the CO and OH peaks by 0.07 eV and a general width increase by ∼0.25 eV. The latter is consistent with the expected small shifts (0.1-0.2 eV) caused by the different registries with the substrate (see SI, section S5) and/or with the shift (0.3 eV) between paired and unpaired carboxyl groups in the protonated state (Figure 3(c)) due to dangling molecular terminations at the rim of the ribbons. The OH and CO

View Article Online
DOI: 10.1039/C7CP06612K

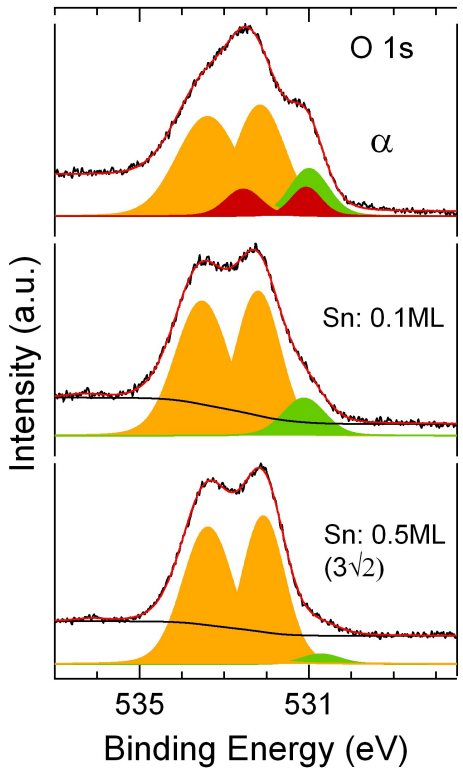

Fig. 4 Quantitative analysis of the O1s spectra already shown in Fig. 2. Bottom: TPA adsorbed on the $3\sqrt{2}$ reconstruction of the Sn/Cu(100) surface alloy. Middle: TPA adsorbed on a 0.1ML Sn/Cu(100) surface alloy. Top: TPA adsorbed on bare Cu(100) substrate. The optimized parameter values are summarized in Table 1. Orange components: OH and CO peaks of the double $[OH\cdots O]$. Red components: OH and CO peaks of the single $[OH\cdots O]$. Green component: carboxylate.

peaks stemming from the protonated group paired to the deprotonated one by a single hydrogen bond display a slightly larger BE separation of ∼1.5 eV, which is also in agreement with the trend predicted by the simulations. Notably, very similar values of the adjusted fitting parameters were obtained for the other two independently-prepared samples (see SI, section S4). Therefore, from our experimental O1s photoemission data set we conclude that the α-phase is composed of both protonated and partially deprotonated molecules.

We can now draw a model of the TPA ribbons of the α phase, where some semiprotonated molecules are intercalated between protonated ones in the ribbons (see Fig. 5). The integrated areas as obtained by the fittings yield a ratio of 6.3:1:1 (75% : 12% : 12%) of carboxylic groups forming double H bonds (OH+CO) to carboxylic groups involved in single H bonds (OH+CO) and to carboxylate groups (COO^-) involved in single H bonds. Each single bonded protonated-semiprotonated molecular pair contributes with the 2 groups directly involved in the single $[OH\cdots O]$ bond and, additionally, with other 2 carboxylic groups forming double bonds. This imply that the population of double bonded protonated-protonated pairs to the population of single bonded protonated-semiprotonated pairs is 4.3 to 4. This means that about half of the molecules are involved in single H bonds.

Interface	O1s	Double $[OH\cdots O]$ CO	Double $[OH\cdots O]$ OH	Single $[OH\cdots O]$ CO	Single $[OH\cdots O]$ OH	Carboxylate
α phase	E_B	532.15	+1.24	531.06	+1.48	530.99
	W_G	1.30	1.61	0.75	0.90	0.99
	Area	36.0 %	39.1 %	5.7 %	6.2 %	**12.0 %**
TPA/ 0.1ML Sn	E_B	532.20	+1.31			531.12
	W_G	1.15	1.38			1.07
	Area	43 %	47 %			**10 %**
TPA/$3\sqrt{2}$	E_B	532.08	+1.31			530.70
	W_G	1.09	1.31			0.97
	Area	46 %	50 %			**3 %**

Table 1 Main parameter values obtained from the fittings of the O1s spectra shown in Figure 4. BE and W_G are expressed in eV. See text for details about the fitting function. The position of the OH peaks is referred to the CO one.

Regarding the C1s peak corresponding to the α phase, it presents a complex line shape with five well resolved peaks at BE of 284, 285, 286.8, 287.9 and 289.3 eV, as seen in Figure 2. Due to the many chemical inequivalent carbons presented in the five-peaks model, establishing a correlation between the observed peaks and the chemically inequivalent C atoms in the proposed carboxyl/carboxylate bond model is not evident. Notice that the single $[OH\cdots O]$ bond implies a highly asymmetrical configuration for the C rings of the two involved molecules. For this reason, we have limited the quantitative analysis to the O1s line shape. We will give, however, a qualitative explanation of the most prominent features in the C1s spectrum of the α phase. From comparison with the C1s spectra obtained from TPA adsorbed on the 0.1ML-Sn/Cu(100) and $3\sqrt{2}$ surfaces, the peaks at 285 and 289.3 eV have to be associated with the contributions of the ring carbons and the carbons of carboxyl groups of complete molecules, respectively. Similarly, the peak at lowest binding energy (284 eV) can be associated with the benzene carbons in the semiprotonated molecules. The shift by ∼ 1 eV to lower BE with respect to the case of complete molecules is consistent with the case of trimesic acid on Cu(110) where a similar shift was reported.[6] Regarding the peak at 286.8 eV, we attribute it to the contribution of the carboxylate groups in the partially deprotonated molecules. Finally, the origin of the peak at ∼288 eV is less clear. We attribute this peak to the contribution of the protonated carboxylic groups involved in single $[OH\cdots O]$ bonds. This implies a shift by ∼1 eV to lower BE with respect to the contribution of the carboxylic groups involved in double $[OH\cdots O]$ bonds , which is comparable to the shift values obtained for the corresponding OH and CO peaks (see Table 1).

Looking at the spectral weight of each component, we observed some discrepancies (e.g. peaks at 286.8 and 288.0 eV should have similar intensity, while they yield a 1:2 ratio). In fact, the overall integrated intensity of the benzene-ring contributions at BE $\geq$ 286.2 eV compared to that of the carboxylic contributions (BE $\leq$ 286.2 eV) yields a ratio of 2.75 instead of 3. This means that the high BE side of the spectrum contains some contributions from satellites of the benzene rings. In addition, photoelectron diffraction effects due to the different adsorption site of each carbon atoms should be also taken into account. In conclusion, the relative intensity of the carbon peaks cannot be rationalized on the basis of simple stoichiometric arguments.

View Article Online
DOI: 10.1039/C7CP06612K

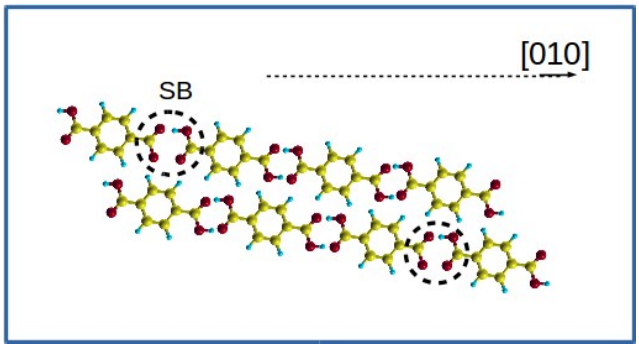

Fig. 5 Model for the α-phase of the TPA/Cu(100) system. The ribbons are composed of both complete and semiprotonated molecules forming an arrangement similar to that of the 2D sheets formed by protonated TPA molecules. On average, half of the molecules are involved in single $[OH\cdots O]$ bonds (dashed circle). The spatial distribution of the single H bonds in the depicted ribbon is arbitrary.

To gain a deeper understanding about the nature of the α phase, we calculated the adsorption energy of the two molecular configurations shown in Figure 3. We found that the calculated energy gain associated to the formation of double H bonds is 0.62 eV. Regarding the single H bonds, we found that they are unfavourable with respect to the double H bonds by 0.46 eV and, therefore, we conclude that they are stable at low temperatures. Thus, once a double H bond is formed, it will not break to form a single H bond. Therefore, the partially protonated molecules should be formed firstly by deprotonation of unpaired carboxylic groups and, then, they would be incorporated in the α-phase by forming single H bonds.

3.3 Modification of TPA self-assembly by Sn surface alloying.

In our former study, we have shown that TPA on the 0.5ML-Sn/Cu(100) surface alloy aggregates into compact domains of protonated molecules that are in registry with the $3\sqrt{2}$ surface reconstruction.[13] However, at coverages lower than ~ 0.1ML , Sn atoms are randomly distributed on the top surface layer,[24] which implies that TPA cannot adopt the same self-assembly mechanism and morphology of the $3\sqrt{2}$ case.

Figure 6 compares the self-assembly morphology of the TPA molecules on the 0.1ML-Sn/Cu(100) surface alloy with those observed on the bare Cu(100). Both surfaces have the same molecular coverages and were prepared at the same substrate low temperature. It is evident that 1D molecular chains are dominant on the modified substrate (Fig.6(a)), whereas only a few of them are observed on the bare substrate. Although quite scattered in direction and length, the 1D chains display a regular intermolecular spacing of 9.5 ± 0.5 Å, which is a characteristic value of TPA molecules connected through straight $[OH\cdots O]$ double bonds,[7,13] in agreement with expectations from the XPS analysis. Additionally, Sn alloying causes an observable increment of the amount of defects of the molecular arrangements. Notice that short straight chains and bent chains are frequent in the image. In the regions of the surface free of molecules, the lateral distribution of embedded Sn atoms can be seen.

The effective inhibition of single $[OH\cdots O]$ bonds with such a low Sn amount may be rationalized in terms of the structural model of Figure 3(d,e) and the local modification of the substrate structure. As discussed in the previous section, one of the two oxygen atoms of the carboxylate remains strongly bonded to a Cu atom whereas the other displaces upwards to approximately the height of the C rings to form the single $[OH\cdots O]$ bond. In the surface alloy, the embedded Sn atoms are displaced outwards by ~ 0.5 Å with respect to the outmost Cu layer,[21] thus increasing also the average vertical distance of any molecule standing above it. The increasing of the vertical distance of the benzene rings with respect to the Cu atoms in the top surface layer, prevents the simultaneous formation of the required $[OH\cdots O]$ and O-Cu bonds nearby a Sn atom. For similar reasons, the random lateral distribution of the Sn embedded atoms is responsible of the frequent bending and scattered orientation of the 1D segments.

The high corrugation of the surface, and hence of the molecule-substrate potential, is even more effective in preventing the formation of a regular network of weak lateral H bonds between molecules in adjacent 1D chains. Thus, the variation of surface corrugation, associated to the randomly distributed low coverage Sn atoms, confine TPA molecules into percolating 1D chains of double $[OH\cdots O]$ bonds.

3.4 Deprotonation as a function of temperature.

The image in Figure 7a, taken at 260K, shows an intermediate stage of the irreversible $\alpha \rightarrow \beta$ phase transition of a TPA/Cu(100) interface prepared at 220K. Domains of the two phases are seen coexisting in the image. This transformation takes place in a narrow temperature range and a small temperature increment of 20K is enough to convert the whole film into the β-phase. This is illustrated by the image of Figure 7b, taken at 280K, where only 2D domains of paired molecular rows aligned along the $< 100 >$ crystallographic directions of the Cu(100) surface are seen[8,12].

The nucleation of the β-phase can be appreciated in better detail in the high resolution image of Figure 7c, where incipient β domains can be compared to the adjacent domains of the α-phase. The β-phase appears to be formed by the fragmentation of the α-phase domains into short segments of paired rows that are the seeds of the β-phase. This molecular re-organization, due to the azimuthal reorientation of TPA molecules,[12] also leads to the disappearance of the long-wavelength modulation of the α phase ribbons. In this regard, we notice that the variation of the apparent molecular height of the α-phase is smoothly changing across multiple molecules, as emphasized in the Z-profiles shown in Figure 7d. This indicates that the long-wavelength modulation cannot be directly associated with some specific structural feature of the single $[OH\cdots O]$ bonds, rather it is likely due to the different registry of the molecules with the substrate lattice.

The corresponding evolution of the O1s and C1s photoemission spectra across the $\alpha \rightarrow \beta \rightarrow \gamma$ phase transformations is shown in Figure 8. In order to prevent kinetic effects due to thermally activated reactions, the sample was heated during 20 sec at the indicated temperature just before measuring XPS. First of all, the integrated intensities of both C1s and O1s spectra were found

View Article Online
DOI: 10.1039/C7CP06612K

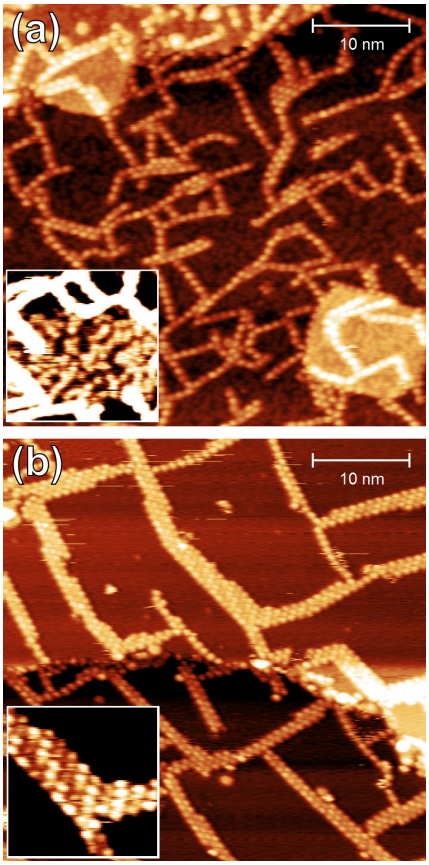

Fig. 6 STM images taken at 130K with -2V/20 pA. (a) TPA molecules deposited on a 0.1ML-Sn/Cu(100) surface alloy held at 180K. Molecular coverage (0.33 $\pm$ 0.05) ML. The inset shows with enhanced contrast a region devoid of molecules in between the molecular chains, where the embedded Sn atoms can be discriminated. (b) TPA molecules deposited on Cu(100) also held at 180K. The inset corresponds to a zoomed image of the ribbons where the modulation stripes are seen more clearly. Coverage: (0.33 $\pm$ 0.05) ML.

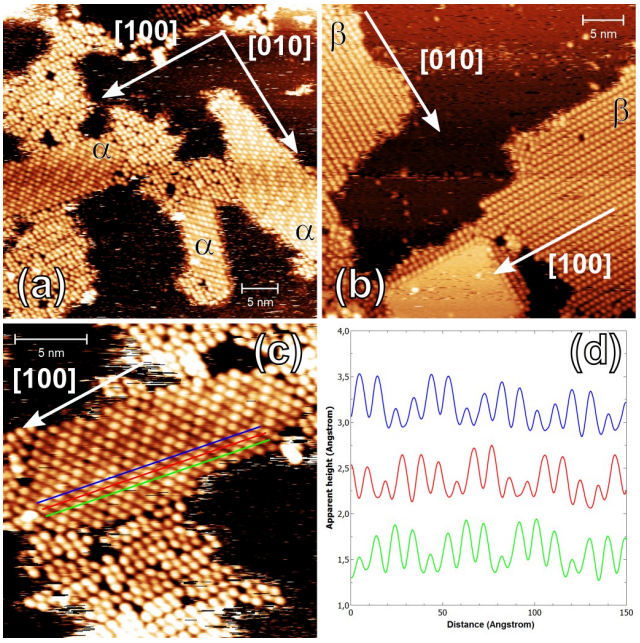

Fig. 7 STM images illustrating the irreversible structural transition from the α-phase into the β one induced by temperature. (a): Surface prepared at $\sim$220K after increasing substrate temperature to 260K. Image taken at the same temperature with (-2V/500 pA) (b): same sample but at 280K (-2V/200pA). The β-phase is observed. (c) STM image taken at 260K (-2V/500pA). The observed modulation stripes are characteristic of the α phase. The color lines indicates the growth direction. (d) Height profiles along three contiguous chains of molecules corresponding to the color lines draw in panel (c).

to be practically constant in the considered temperature range, pointing to a negligible molecular desorption from the α to the γ-phase. Then, we can notice that the XPS changes are very small from 228 K to 273 K, while a sharp rising of the O1s carboxilate component at 531 eV takes place between 273 K and 293 K. The heating experiment ended at 381K with a typical spectra of the 3×3 phase.

Finally, we compared the kinetics of the deprotonation reaction on the bare Cu(100) surface and on the 0.1ML-Sn/Cu(100) surface alloy. To this aim, we measured the O1s spectra in real time during heating at a 40K/min rate in snapshot acquisition mode on the two surfaces. The corresponding temperature variation of the relative weight of the carboxylate component is shown in Figure 9. The general slope of the carboxylate temperature dependence on the bare Cu(100) surface resembles those previously reported for other carboxylic acids on the Cu(100) surface,[32,33] where a steep rise is observed close to RT. In this case, however, the deprotonation curve has not a steady slope, but it presents well defined features. The amount of carboxylates remains practically constant from 230 K up to $\sim$ 290 K, where it starts to increase steeply. From comparison with the STM images (Fig. 7) and the XPS spectra (Fig. 8) , we associate the initial plateau to the activation barrier increase related to the formation of the α-phase, and the drastic change of slope observed at 290K to the transformation of the α-phase into the β one. Similarly, we attribute the sharp step edge at $\sim$ 320 K to the stabilization of the β phase. After a narrow plateau associated with the thermal stability of the β phase[12], the amount of carboxylates monotonically increases up to $\sim$ 380 K , where all the adsorbed molecules become deprotonated. This third and last plateau reflects the formation of the fully deprotonated (3×3) phase. We remark that the transition temperatures from one structural phase to the next one derived from this experiment are higher than those derived from the variable-temperature STM experiments and steady-temperature XPS (see Figure 7). This is due to the fast heating/rate used in the snapshot experiment combined with the mounting setup of the sample at ALOISA: the thermocouple is not in direct contact with the sample, but with a Mo spacer below the sample, thus determining a heat-load impedence during variable temperature experiments. Nonetheless, the occurrence of well defined plateaus in the carboxylate curves allows us to unequivocally identify the different TPA phases.

In the case of the Sn-alloyed surface, the increase of carboxylates sets in already at the lowest considered temperature (see Fig. 9). The increase of carboxylate now displays an almost steady slope up to the full conversion into a deprotonated phase

View Article Online
DOI: 10.1039/C7CP06612K

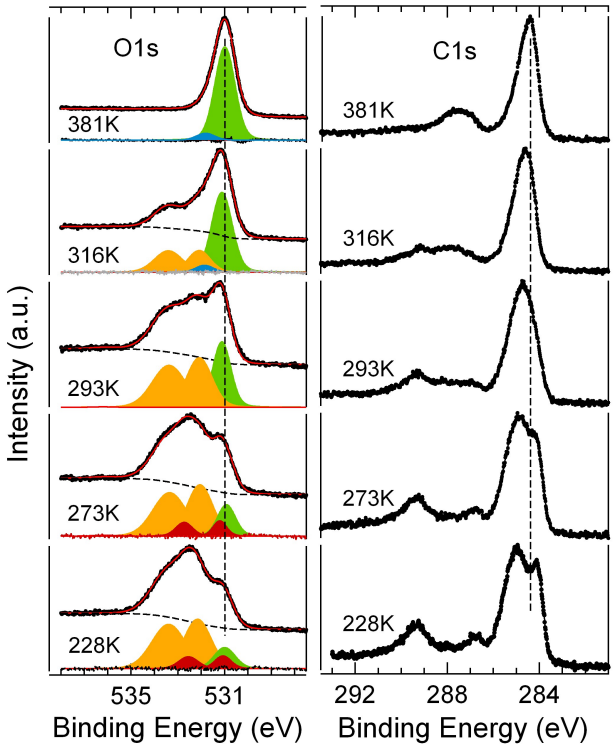

Fig. 8 Evolution of the O1s and C1s photoemission spectra (left and right panels, respectively) as a function of temperature of a 0.38 ML coverage of TPA deposited at ∼230K. See text for experimental details of the heating procedure. The small extra component (blue shaded curve, 7% of the total intensity) in the O1s spectrum of the γ-phase effectively accounts for the observed asymmetry of the carboxylate peak, a characteristic of terephthalates observed also on Cu(110).[11]

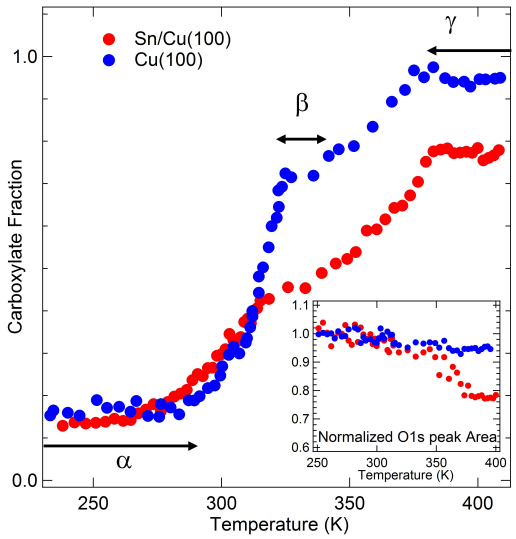

Fig. 9 Fraction of carboxylates relative to the total intensity of the initial O1s peaks, as a function of substrate temperature, for both the bare Cu(100) and the 0.1ML-SnCu(100) surfaces. The arrows indicate the thermal stability range of the α, β and γ phases as discussed in the text. See text for details. The inset shows the total area of O1s peak normalized with respect to the total intensity of O1s peak obtained from each sample as prepared.

at 380 K, thus smearing both the LT plateau and the intermediate one corresponding to the β-phase on the bare Cu(100) surface. This strongly suggests the existence of a multiplicity of activation energy barriers for deprotonation due to the intrinsic disorder of the Sn-alloyed surface. In particular, we attribute the observed increase of carboxylates in the low-temperature range (from 230 to ∼290K) to the occurrence of unpaired and poorly coordinated carboxylic groups (e.g. associated with the frequent bending of the 1D chains, see Fig. 6(a)) since they should have a lower activation barrier than carboxylic groups involved in well-formed $[OH\cdots O]$ bonds. Finally, the amount of carboxylate on the surface alloy saturates at the same temperature (375-385 K) as in the case of the Cu(100) surface. However, the saturation value is only ∼80 % of the initial amount of molecules. This is due to the opening of the molecular desorption channel at 350K (see the inset). Indeed, about 20% of the molecules desorbes from the surface in the temperature range between 350 and 375 K. We note that the temperature range where molecular desorption take place is the same as that observed in the TPA/$3\sqrt{2}$ case[13], which suggests that the desorbed molecules are complete molecules coming from regions of the surface with a lower local reactivity due to a higher local density of Sn atoms.

4 Conclusions

We showed that both the O1s and the C1s photoemission peaks of the LT α-phase of TPA on Cu(100) are not compatible with a molecular layer made of fully protonated TPA molecules connected through double $[OH\cdots O]$ bonds, as reported in former models.[8] We proved the presence of a significant fraction of deprotonated molecules from comparison with XPS spectra measured on the fully deprotonated γ-phase and films grown on Sn-alloyed surfaces that prevent molecular deprotonation. By means of DFT based simulation of the O1s core level photoemission, we demonstrated that the most plausible scenario is described by the formation of a single hydrogen bond $[OH\cdots O]$ between the carboxylic group of a protonated TPA with the carboxylate group of a semiprotonated TPA. In this model, the molecular structure of the observed ribbons is similar to that of the 2D sheets formed by protonated TPA molecules on inert surfaces such as Au(111) and on the $3\sqrt{2}$ reconstruction of the Sn/Cu(100) surface alloy, but with an approximately one to one population of single bonded protonated-semiprotonated TPA pairs to double bonded protonated-protonated pairs. A comparative analysis of the energetics related to the formation of single and double H bonds on the Cu(100) surface indicates that the semiprotonated molecules are generated by the deprotonation of unpaired carboxylic groups. Once a semiprotonated molecule is formed, it is incorporated in the α-phase by forming a single H bond. This novel motif of hydrogen bonding could be exploited in supramolecular architectures based on two carboxylic-acid species with different deprotonation probabilities.[34] Finally, by monitoring the kinetics of the deprotonation reaction, we showed that the intercalation of the semiprotonated molecules

View Article Online
DOI: 10.1039/C7CP06612K

into a regular network of H bonds does not weakens the activation barrier for further deprotonation on the Cu(100) surface, whereas it takes place at ~ 50 K lower temperature for isolated or poorly coordinated protonated molecules on the 0.1ML-Sn/Cu(100) passivated surface.

5 Conflicts of interest

There are no conflicts of interest to declare.

6 Acknowledgments

Five of us, J.D.F., L.J.C, L.M.R., J.E.G. and H.A. are members of CONICET of Argentina. We also thank CONICET for the fellowships of B.Q.A.. We thank Mr. Lucas López for valuable technical assistance. We acknowledge financial support by the following Argentine institutions: CONICET (PIP -2015-00274), ANPCYT (PICT-2015-0922), UNCuyo(06/C498). We also acknowledge financial support from the ICTP-ELETTRA USERS PROGRAMME. We thank the Centro de Simulación Computacional p/Aplicaciones Tecnológicas (CSC-CONICET) for granting the use of computational resources which allowed us to perform part of the simulations included in this work.

References

1 S. Stepanow, N. Lin, F. Vidal, A. Landa, M. Ruben, J. Barth and K. Kern, *Nano Lett.*, 2005, **5**, 901–904.
2 M. Lackinger and W. Heckl, *Langmuir*, 2015, **25**, 11307–11321.
3 S. Stepanow, R. Ohmann, F. Leroy, N. Lin, T. Strunskus, C. Wöll and K. Kern, *ACS Nano*, 2010, **4**, 1813–1820.
4 R. Gutzler, S. Stepanow, D. Grumelli, M. Lingenfelder and K. Kern, *Acc. Chem. Res.*, 2015, **48**, 2132–2139.
5 J. Urgel, B. Cirera, Y. Wang, W. AuwÃd'rter, R. Otero, J. Gallego, M. Alcamí, S. Klyatskaya, M. Ruben, F. Martín, R. Miranda, D. Ecija and J. Barth, *Small*, 2015, **47**, 6358–6364.
6 T. Classen, M. Lingenfelder, Y. Wang, R. Chopra, C. Virojanadara, U. Starke, G. Contantini, G. Fratesi, S. Fabris, de Gironcoli S. and et.al., *J. Phys. Chem. A*, 2007, **111**, 12589–12603.
7 S. Clair, S. Pons, A. P. Seitsonen, H. Brune, K. Kern and J. Barth, *J. Phys. Chem. B*, 2004, **108**, 14585–14590.
8 S. Stepanow, T. Strunskus, M. Lingenfelder, A. Dmitriev, H. Spillmann, N. Lin, J. Barth, C. Wöll and K. Kern, *J. Phys. Chem. B*, 2004, **108**, 19392–19397.
9 M. E. Cañas-Ventura, F. Klappenberger, S. Clair, S. Pons, K. Kern, H. Brune, T. Strunskus, C. Wöll, R. Fasel and J. V. Barth, *The Journal of Chemical Physics*, 2006, **125**, 184710.
10 Y. Ge, H. Adler, A. Theertham, L. L. Kesmodel and S. L. Tait, *Langmuir*, 2010, **26**, 16325–16329.
11 Y. Wang, S. Fabris, T. White, F. Pagliuca, P. Moras, M. Papagno, D. Topwal, P. Sheverdyaeva, C. Carbone, M. Lingenfelder, T. Classen, K. Kern and G. Costantini, *Chem. Commun.*, 2012, **48**, 534–536.
12 J. Fuhr, A. Carrera, N. Murillo-Quirós, L. J. Cristina, A. Cossaro, A. Verdini, L. Floreano, J. E. Gayone and H. Ascolani, *J. Phys. Chem. C*, 2013, **117**, 1287.
13 A. Carrera, L. J. Cristina, S. Bengió, A. Cossaro, A. Verdini, L. Floreano, J. D. Fuhr, J. E. Gayone, and H. Ascolani, *J. Phys. Chem. C*, 2013, **117**, 17058.
14 D. Schwarz, R. van Gastel, H. Zandvliet and B. Poelsema, *J. Phys. Chem C*, 2013, **117**, 1020–1029.
15 D. Schwarz, R. van Gastel, H. Zandvliet and B. Poelsema, *Phys. Chem. Chem. Phys.*, 2013, **15**, 5007–5016.
16 J. Schnadt, W. Xu, R. Vang, J. Knudsen, Z. Li, E. Lægsgaard and F. Besenbacher, *Nano Res*, 2010, **3**, 459–471.
17 T. Schmitt, L. Hammer and M. Schneider, *J. Phys. Chem. C*, 2016, **120**, 1043–1048.
18 M. Franke, F. Marchini, L. Zhang, Q. Tariq, N. Tsud, M. Vorokhta, M. Vondrá, K. Prince, M. Röckert, F. Williams, H.-P. Steinrück and O. Lytken, *J. Phys. Chem. C*, 2015, **119**, 23580–23585.
19 M. Lingenfelder, H. Spillmann, A. Dmitriev, S. Stepanow, N. Lin, J. V. Barth and K. Kern, *Chem. Eur. J.*, 2004, **10**, 1913–1919.
20 J. Martínez-Blanco, V. Joco, T. Balasubramanian, P. Segovia and E. G. Michel, *App. Surf. Sci.*, 2006, **252**, 5331.
21 J. D. Fuhr, J. E. Gayone, J. Martínez-Blanco, E. G. Michel and H. Ascolani, *Physical Review B*, 2009, **80**, 115410.
22 R. Gotter, A. Ruocco, A. Morgante, D. Cvetko, L. Floreano, F. Tommasini and G. Stefani, *Nucl. Instrum. Methods Phys. Res. A*, 2001, **467**, 1468–1472.
23 L. Floreano, G. Naletto, D. Cvetko, R. Gotter, M. Malvezzi, L. Marassi, A. Morgante, A. Santaniello, A. Verdini, F. Tommasini and et.al., *Rev. Sci. Instrum.*, 1999, **70**, 3855–3865.
24 P. Machaín, J. E. Gayone, J. D. Fuhr and H. Ascolani, *Applied Surf. Science*, 2017, **422**, 838–846.
25 G. Cautero, R. Sergo, L. Stebel, P. Lacovig, P. Pittana, M. Pedronzani and S. Carrato, *Nucl. Instrum. Methods Phys. Res. A*, 2008, **595**, 447–459.
26 P. Giannozzi, S. Baroni, N. Bonini, M. Calandra, R. Car, C. Cavazzoni, D. Ceresoli, G. L. Chiarotti, M. Cococcioni, I. Dabo and et.al., *J. Phys.: Condens. Matter*, 2009, **21**, 395502.
27 O. A. Vydrov and T. van Voorhis, *J. Chem. Phys.*, 2010, **133**, 244103.
28 R. Sabatini, T. Gorni and S. de Gironcoli, *Phys. Rev. B*, 2013, **87**, 041108(R).
29 A. Cossaro, M. Puppin, D. Cvetko, G. Kladnik, A. Verdini, M. Coreno, M. de Simone, L. Floreano and A. Morgante, *J. Phys. Chem. Lett.*, 2011, **2**, 3124–3129.
30 A. Cossaro, D. Cvetko and L. Floreano, *Phys. Chem. Chem. Phys.*, 2012, **14**, 13154–13162.
31 S. Tait, Y. Wang, G. Costantini, N. Lin, A. Baraldi, F. Esch, L. Petaccia, S. Lizzit and K. Kern, *J. Am. Chem. Soc.*, 2008, **130**, 2108–2110.
32 B. Immaraporn, P. Ye and A. Gellman, *J. Chem. Phys.*, 2000, **112**, 3351 –3357.
33 B. Immaraporn, P. Ye and A. Gellman, *J. Phys. Chem. B*, 2004, **108**, 3504–3511.
34 X. Bouju, C. Mattioli, G. Franc, A. Pujol and A. Gourdon, *Chemical Reviews*, 2017, **117**, 1407–1444.